Journal of Materials Chemistry C

PAPER

View Article Online
View Journal | View Issue

Cite this: J. Mater. Chem. C, 2017, 5, 601

Fluorescence turn-on detection of uric acid by a water-stable metal–organic nanotube with high selectivity and sensitivity†

Xuelian Xin,[ab] Minghui Zhang,[b] Jianwei Zhao,[c] Chengyou Han,[b] Xiuping Liu,[b] Zhenyu Xiao,[b] Liangliang Zhang,[b] Ben Xu,[b] Wenyue Guo,[b] Rongming Wang*[ab] and Daofeng Sun*[ab]

Received 20th November 2016,
Accepted 13th December 2016

DOI: 10.1039/c6tc05034d

www.rsc.org/MaterialsC

Herein we provide a new strategy for fluorescence detection of uric acid (UA) using a metal–organic nanotube of **CD-MONT-2** for the first time. This novel fluorescent probe exhibits high selectivity and sensitivity for UA with a very good detection limit of 4.3 μM. The results of density functional theory calculations and ^{1}H NMR spectra show that the turn-on sensing mechanism arises from the host–guest interactions of capsule-like **CD-MONT-2** with UA to result in electron transfer between UA and **CD-MONT-2′**. Furthermore, **CD-MONT-2′** exhibits very fast adsorption of UA molecules in aqueous solution as confirmed by UV-Vis spectra and HPLC analysis, making it a potential candidate for application in the removal of UA from the human blood.

1. Introduction

The presence of uric acid (UA) in the blood is one of the key factors affecting our physical health.[1–3] Elevated levels of UA lead to numerous diseases, for instance, hyperuricemia, gout, renal failure, physiological disorders and Lesch–Nyhan syndrome, and lower UA levels cause Wilson's disease.[4–7] Recently, a few methods for detection of UA have been reported, including electrochemical analysis (EA), high performance liquid chromatography (HPLC), spectrophotometry, fluorescence method (FL) and chemiluminescence.[8–10] However, most of the these methods are time-consuming and have costly instrumentation requirements and finite selectivity; for example, the HPLC method always requires a tedious sample preparation procedure and complicated maintenance.[3] Therefore, it is crucial to develop rapid and precise methods to identify the UA levels.

Host–guest chemistry is a selective combination between host (or receptor) and guest (or substrate) with H-bond donor/acceptor, oppositely charged groups, covalent bonds, supramolecular systems, *etc.* As a consequence, the combination can generate either electron transfer or energy transfer between the guest and the host (the mechanism is shown in Fig. 1).[11–14] This phenomenon was also utilized in UA detection using the host of cyclodextrins due to their capsule-like shape.[15] The cyclodextrins have been widely used in biomedical fields because of the cone-shaped cavity, nontoxicity and stability in water.[16] Very recently, Liu *et al.* introduced a carbon nanotube (CNT) ionic liquid paste electrode which was modified with electropolymerized poly(β-cyclodextrin). Their results suggest that porous β-cyclodextrin has a remarkable selectivity for UA due to the ''host–guest'' recognition.[17] Unfortunately, the detailed recognition mechanism

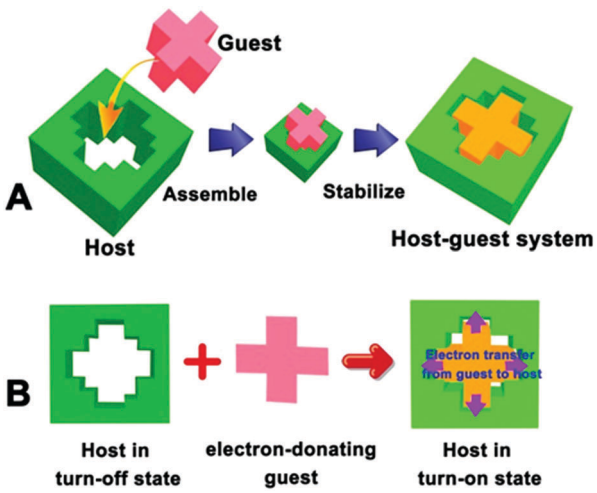

Fig. 1 Mechanism of host–guest systems ((A) the selective combination between host and guest; (B) interaction between host and guest).

[a] State Key Laboratory of Heavy Oil Processing, China University of Petroleum (East China), Qingdao Shandong 266580, China. E-mail: rmwang@upc.edu.cn, dfsun@upc.edu.cn
[b] College of Science, China University of Petroleum (East China), Qingdao 266580, China
[c] College of Chemical Engineering, China University of Petroleum (East China), Qingdao 266580, China

† Electronic supplementary information (ESI) available. See DOI: 10.1039/c6tc05034d

and the action sites between the poly(β-cyclodextrin) and UA molecules were unclear due to the fact that the complex composite structure makes it difficult for further characterization.[18]

Metal–organic nanotubes, as a new type of functional materials, have been utilized in the fields of fluorescence, catalysis, and gas adsorption/separation.[19] The capsule-like shape of a metal–organic nanotube implies its potential application in UA detection based on host–guest interactions,[20] and its excellent crystalline property also favors the accurate characterization of host–guest interactions and the detailed study of the recognition mechanism.[21] Herein, we suggest a highly selective and sensitive strategy for detection of UA based on its host–guest interactions with the Pb(II)-based metal–organic nanotube of **CD-MONT-2′** (the guest-free form of **CD-MONT-2**), demonstrating that the detection accuracy and efficiency are significantly improved.[22,23]

2. Results and discussion

2.1 Structural description and detective performance of CD-MONT-2′

The synthesis strategy of **CD-MONT-2** is depicted in the experimental section. The dimensions of chiral cavities in an as-prepared **CD-MONT-2** are about 13.0 × 10.3 × 10.2 Å with cyclohexanol molecules filling inside, as shown in Fig. S1 (ESI†).[24] The guest cyclohexanol molecules were removed by heating the sample of **CD-MONT-2** at a temperature of 120 °C for 1 hour to obtain the guest-free form, **CD-MONT-2′** (the powder X-ray diffraction patterns [PXRD] are shown in Fig. S2, ESI†). Subsequently, the **CD-MONT-2′** is ground and put into H_2O and subjected to ultrasonication for one hour until a homogeneous suspension (1 mg mL^{-1}) is achieved. H_2O is employed due to its non-toxicity and non-reactivity towards **CD-MONT-2**.[25] The fluorescence titration is performed by gradually adding the UA to the **CD-MONT-2′** suspension with fluorescence emission at 526 nm upon excitation at 330 nm.[26] As shown in Fig. S3 (ESI†), initially the **CD-MONT-2′** suspension only exhibits weak fluorescence, indicating a "turn-off" state. With gradual addition of the UA solution (1 mmol L^{-1} in H_2O), a drastic increase of fluorescence intensity is observed, indicating its sensitivity to UA. Almost 17-fold fluorescence enhancement is observed to achieve the fluorescence "turn-on" state of **CD-MONT-2′** after adding 20 μM UA (Fig. 2a). The experiments are repeated 3 times. The fluorescence recovery efficiency changes in proportion to the square root of the concentration of UA, according to the square root calibration equation $(I - I_0)/I_0 = 4.95\sqrt{c} - 5.8$ shown in Fig. 2b (where I_0 is the initial fluorescence intensity, I is the fluorescence intensity after the addition of analyte).[27–35] The LOD accounts for the lowest concentration of analyte that can be determined reproducibly, and it is calculated by the following equation: LOD = $k \times \sigma/S$, where k, σ, and S are

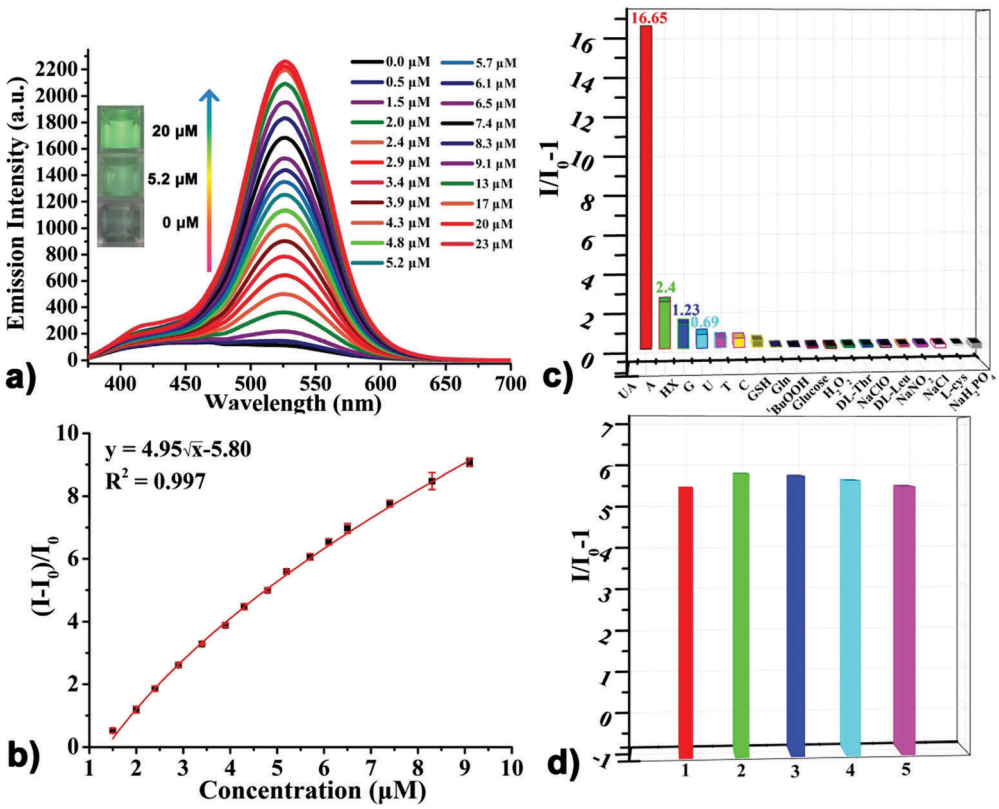

Fig. 2 (a) Fluorescence spectra of 1 mg mL^{-1} **CD-MONT-2′** in H_2O treated with continual addition of UA, and the inset pictures are taken under a Xe lamp at a concentration of 0, 5.2 and 20 μM. (b) Effect of the concentration of UA on fluorescence recovery efficiency. (c) Fluorescence intensity of $I/I_0 - 1$ (526 nm) spectra with 20 μM UA, purines, pyrimidines, 50 μM inorganic salts, reducing agents, amino acids, RNS and ROS, respectively. (d) Interference experiments with 1 (5.2 μM UA), 2 (5.2 μM UA + 5.2 μM A), 3 (5.2 μM UA + 5.2 μM T), 4 (5.2 μM UA + 20.8 μM C) and 5 (5.2 μM UA + 5.2 μM A + 20.8 μM C).

the confidence level parameter, the standard deviation of blank test values, and the sensitivity of the fluorescence peak towards analyte concentration, respectively. In this scenario, the k value of 3, the σ value of 7.10 (calculated from 11 groups of blank test), and the S value of 4.95 (based on the nonlinear regression in the range of 1.5 to 9.1 μM) are used for the equation. Accordingly, the LOD values are calculated to be 4.3 μM.[20,36–38] The LOD value presented here indicates a good performance among the reported results on fluorescence detection of UA, indicating the high sensitivity (Table S1, ESI†).

To further evaluate the selectivity of **CD-MONT-2′** to UA, the fluorescence detection of other substances is also carried out and the results are illustrated in Fig. 2c and Fig. S4 (ESI†). Purines (hypoxanthine [HX], adenine [A], and guanine [G]), pyrimidines (thymine [T], cytosine [C], and uracil [U]), amino acids (GSH, L-cys, Gln, DL-Thr, and DL-Leu), glucose, reactive nitrogen species (NO^{2-}) and reactive oxygen species (H_2O_2 and ^{t}BuOOH), and several inorganic salts (NaCl, NaClO, NaH_2PO_4, *etc.*) are selected as the counterparts. The fluorescence responses to them were tested. No significant fluorescence change was observed when the substances mentioned were gradually added into the emulsion. Three concentrations (5.2, 9.1 and 20 μM) of UA are compared with the same concentration of purines and pyrimidines and excess amounts of other substances. Based on the results, all other substances exhibited an extremely weak influence on **CD-MONT-2′**. At the concentration of 20 μM, the fluorescence enhancement caused by UA (16.65-fold) is much larger than that due to other compounds (all below 2.40-fold), which indicated that the potential substances can hardly produce a distinct influence on the intensity of **CD-MONT-2′**.[39–42] The structures and fluorescence spectra of purines and pyrimidines, and full spectra of titration experiments are shown in Fig. 3 and Fig. S5–S7 (ESI†), respectively. The interference tests (Fig. S8, ESI†) are also performed in order to illustrate the negligible effects of those substances (A, T and C) on the fluorescence intensity of **CD-MONT-2′**. Compared with the spectrum of solution with the addition of only UA, the spectrum of other solutions with the addition of mixed analytes shows little change in fluorescence intensity. The results indicate that the potential substances can hardly produce distinct interference for the detection of UA. Our results suggest that **CD-MONT-2′** possesses high selectivity and sensitivity to UA molecules, implying its remarkable fluorescence "turn-on" response.

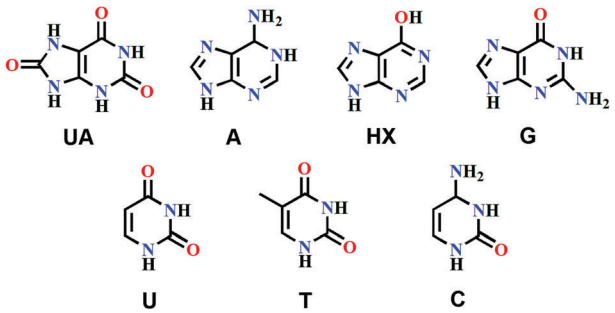

Fig. 3 The structures of UA, A, HX, G, U, T and C.

2.2 Sensing mechanism and density functional theory (DFT) calculations

The apparent response of **CD-MONT-2′** to purines and pyrimidines, particularly to UA, prompted us to explore the detailed recognition mechanism. It is known that host–guest interactions play a key role in fluorescence detection. We suggest that the mechanism is associated with the weak interactions through a process of host–guest interactions (Fig. 4, take UA for example). Based on the structures of guest molecules and **CD-MONT-2′**, we suggest that the guest molecules can be captured by the host through the following four ways: (a) electrostatic interactions between O atoms with lone pairs in guest molecules and uncovered Pb(II) atoms of **CD-MONT-2′**,[43] (b) van der Waals interactions between guest molecules and **CD-MONT-2′** molecules, (c) hydrophobic effect: interactions between the hydrophobic cavity of **CD-MONT-2′** and guest molecules, and (d) hydrogen-bonding interactions between N–H (or O–H in HX) groups of guest molecules and O atoms of **CD-MONT-2′**.[11–13,44] As an electron rich species, the UA molecule could enhance fluorescence intensity, possibly due to its ability to donate electrons from an excited state to the lowest unoccupied molecular orbital of **CD-MONT-2′**. The host–guest interactions result in the connection between electron-donating groups of UA and fluorescent **CD-MONT-2′**. Thus the electron transfer between UA and **CD-MONT-2′** leads to fluorescence enhancement.[6]

Density functional theory (DFT) calculations are performed to evidence the capture and sensing mechanisms of **CD-MONT-2′** for UA employing the program package of DMol^3 in Materials Studio (calculation method is shown in Experimental section).[45,46] The adsorption energies of **CD-MONT-2′** with UA, A, HX and C, and β-cyclodextrin with UA are calculated for comparison. The calculated results are presented in Fig. 5 and Fig. S9 (ESI†), respectively. The calculated interaction energies of UA, A, HX and U in **CD-MONT-2′** are 0.861, 0.832, 0.731 and 0.691 eV, respectively. In contrast, the energy of UA in β-cyclodextrin is 0.520 eV, which is extremely small. The exceptionally high value of UA indicates that **CD-MONT-2′** can preferably capture it.

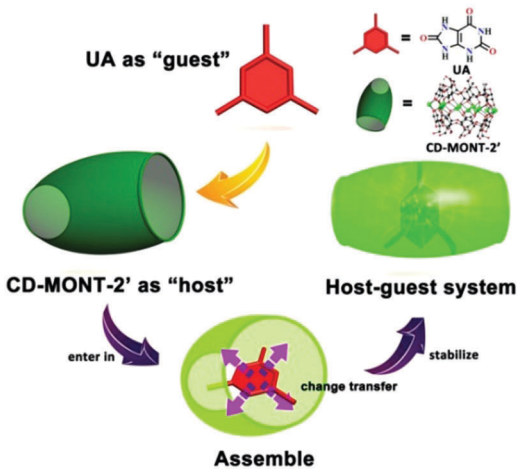

Fig. 4 Schematic diagram of the sensing mechanism for detection of UA by **CD-MONT-2′**.

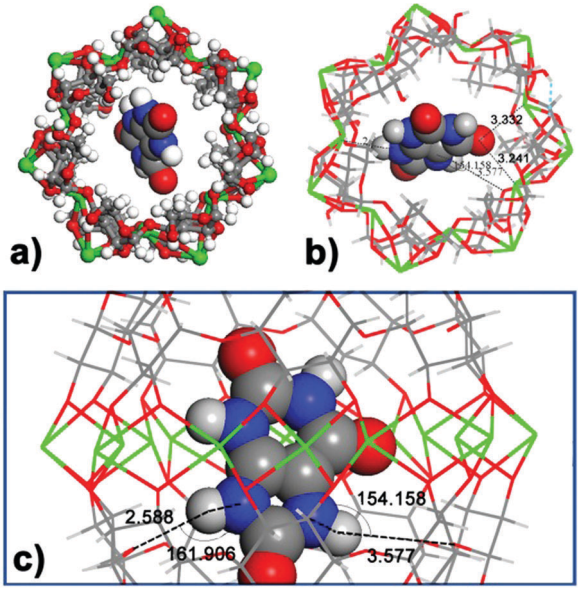

Fig. 5 Structures of (a) the UA molecule inside the pore of **CD-MONT-2′** with the distance and angles marked (b) Pb(II)–O and (c) hydrogen-bonding (green: Pb(II), gray: C, red: O, and light grey: H).

2.3 ^{1}H NMR, UV-Vis spectra, HPLC, FTIR and TGA analysis of the sensing mechanism

To further confirm the aforementioned sensing mechanism, ^{1}H NMR spectra of **CD-MONT-2′**, UA and **UA@CD-MONT-2′** are applied to track the host–guest interactions. Compared with the spectra of UA and **CD-MONT-2′**, the peaks in the spectrum (Fig. 6a) of the inclusion complex formed by **CD-MONT-2′** and UA at δ = 11.74, 11.31, 10.73 and 10.51 ppm disappear, which are assigned to the H atoms of UA, and the new peaks at δ = 10.09, 7.99 and 7.65 ppm appear, which are attributed to the hydrogen-bonding interactions between UA and **CD-MONT-2′**. The above illustrations are also confirmed by a 2D NOESY spectrum of the inclusion complex. The protons H_3 and H_5 of **CD-MONT-2′** molecules show correlations with protons H of UA, suggesting that UA is included into the cavity of the metal–organic nanotube (Fig. 6b, the inset shows the H position in **CD-MONT-2′**).[47]

The host–guest interactions between **CD-MONT-2′** and UA further prompted us to test the possibility of the removal of UA by **CD-MONT-2′** in aqueous solution. Thus, UA was dissolved in water (1 mmol L^{-1}), to which **CD-MONT-2′** (1 mg mL^{-1}) was added. The residual of UA molecules in the solution was detected by UV-Vis spectra and HPLC analysis. The results suggest that with the increase of time, the amount of UA shows a significant decrease, which clearly suggests that the UA molecules are captured by **CD-MONT-2′**. Within 15 min, 77.1% of UA molecules were adsorbed into the pores of **CD-MONT-2′**, as shown in Fig. 7, Fig. S10 and Table S2, ESI,† [48,49] indicating that **CD-MONT-2′** exhibits very fast capture of UA molecules through host–guest interactions and thus possesses potential for application in the removal of UA molecules from the human blood. In addition, the powder X-ray diffraction (PXRD) patterns, FTIR spectra and TGA of **CD-MONT-2′** before and after treatment with UA were also analysed. The purity of the bulk sample was confirmed by powder X-ray diffraction (PXRD) patterns of the as-synthesized, activated sample and **UA@CD-MONT-2′** (Fig. S11, in ESI†), which matched well with the simulated PXRD pattern from the single-crystal data. In the FT-IR spectra (Fig. S12, ESI†), the absorption peaks remain unchanged, except that there are some slight differences. In **UA@CD-MONT-2′**, the peaks around 3406 cm^{-1} and 1384 cm^{-1} show red shift compared with 3389 cm^{-1} and 1369 cm^{-1} in **CD-MONT-2′**, and there are 4 small new peaks at

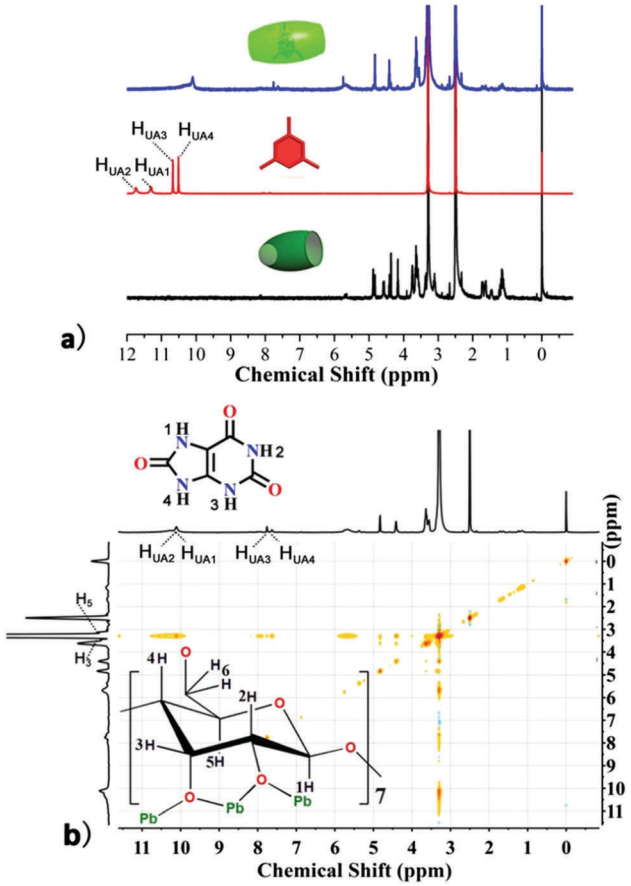

Fig. 6 (a) The ^{1}H NMR spectra of **CD-MONT-2′**, UA and **UA@CD-MONT-2′** in d_6-DMSO. (b) 2D NOESY of **UA@CD-MONT-2′** in d_6-DMSO.

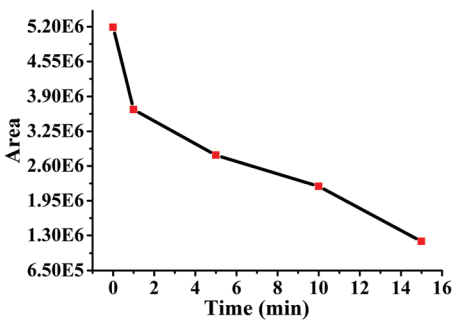

Fig. 7 HPLC analysis of UA adsorbed by **CD-MONT-2′** at the retention time of UA standard 8.7 min.

2976, 1540 (C=O), 880 and 679 cm^{-1}.[50] The differences come from the weak interactions of UA and **CD-MONT-2′**, which agree with the results of ^{1}H NMR spectra. Thermogravimetric analysis (TGA) show that the samples of **CD-MONT-2′** and **UA@CD-MONT-2′** are stable until 270 °C, and the smoothness may come from the lower crystallinity when UA molecules enter into the cavities (Fig. S13, ESI†).

3. Conclusions

In summary, a novel fluorescence detection technique of UA is developed for the first time based on a metal–organic nanotube of **CD-MONT-2**. This fluorescent probe can detect UA through fluorescence turn-on with high selectivity and sensitivity. The detection limit is 4.3 μM in the range of 1.5 to 9.1 μM, which makes **CD-MONT-2** one of the best fluorescent probes for UA molecules to date. The sensing mechanisms arise from the host–guest interaction of UA with the capsule-like **CD-MONT-2**, and are quite different from the previous reports. Last but not the least, **CD-MONT-2** is non-toxic and completely bio-friendly, which is of significance for its application in medical and clinical research. Our study provides a novel way for the design and application of new functional materials for fluorescence turn-on detection of UA.

4. Experimental

4.1 Materials and the synthesis strategy

All chemicals and solvents are purchased and used as received without further purification. ^{t}BuOOH could be used to induce ROS. $PbCl_2$ (0.80 mmol, 0.2250 g) and β-CD (0.10 mmol, 0.1150 g) are suspended in 30 mL of distilled water, and then stirred at 80 °C for an hour. The mixture is cooled to room temperature and filtered. The obtained solution is transferred into glass tubes, and then cyclohexanol and trimethylamine are layered on the solution. The glass tubes are sealed and heated at 110 °C for 3 days. A lot of colourless rod-like crystals are collected by filtration (yield: 75%).

4.2 Physical measurements

Fluorescence spectra are recorded using a Hitachi F-7000 fluorescence spectrophotometer. Powder X-ray diffraction data are obtained on a Philips X′ Pert with Cu-Kα radiation (λ = 0.15418 nm). The optical absorption spectra are measured on a UV-vis spectrometer (Specord 205, Analytik Jena) in the range of 200 to 600 nm. The HPLC analysis is performed using a liquid chromatograph (Hitachi LC-20A, Japan), a LC-20A pump, and a SPD-20A UV detector. A C18 column (100 × 4.6 mm i.d., 5.0 μm, Waters) is used at a flow rate of 1.0 mL min^{-1} and 25 °C. Isocratic elution is performed using a mobile phase of phosphate buffer (pH 2.5)–methanol (60 : 40 v/v). The run time is 15.0 min. A UV detector is used to monitor the samples at 254 nm. The injection volume is 20 μL. Analytical software (Primaide) is used for system control and data processing. ^{1}H NMR spectra are recorded on a Bruker AVANCE-400 NMR Spectrometer in d_6-DMSO. FTIR spectra are collected on a Bruker VERTEX-70 spectrometer in the 4000–600 cm^{-1} region.

4.3 Fluorescence experiments

All fluorescence measurements are carried out at room temperature. Samples are excited at 330 nm with the excitation and emission slit widths at 20 and 10 nm, respectively. The emission spectrum is scanned from 350 to 700 nm at a scan rate of 1200 nm min^{-1}. The photomultiplier voltage is set at 400 V.

4.4 Calculation method

Density functional theory (DFT) calculations are performed using the program package DMol^3 in Materials Studio of Accelrys Inc. The exchange correlation energy is calculated with the generalized gradient approximation (GGA) using the form of functional proposed by Perdew and Wang usually referred to as Perdew–Wang 91 (PW91). To take the relativity effect into account, the density functional semicore pseudopotential (DSPP)[6] method is employed for the Pb(II) atoms, and the carbon, oxygen, and hydrogen atoms are treated with an all-electron basis set. The valence electron functions are expanded into a set of numerical atomic orbitals by a double-numerical basis with polarization functions (DNP). Fermi smearing of 0.005 hartree and a real space cutoff of 5.2 Å are used to improve the computational performance. The tolerances of energy, gradient, and displacement convergence are 2×10^{-5} Hartree, 4×10^{-3} Hartree per Å, and 5×10^{-3} Å, respectively. The adsorption energies (ΔE_{ad}) of UA, HX and C interaction with the frameworks of **CD-MONT-2′** are calculated by $\Delta E_{ad} = E_{UA} + E_{\text{CD-MONT-2′}} - E_{\text{UA–CD-MONT-2′}}$, where E_{UA}, $E_{\text{CD-MONT-2′}}$ and $E_{\text{UA–CD-MONT-2′}}$ are the total energies of the UA molecule, the 14-Pb(II)-ring and the adsorption system at their optimized geometries.

Competing financial interests

The authors declare no competing financial interest.

Author contributions

X. L. X., D. F. S. and R. M. W. conceived and designed the experiments and co-wrote the paper. M. H. Z. and Z. Y. X. synthesized the compound. X. L. X., J. W. Z. and L. L. Z. performed most of the experiments and analyzed the data. B. X., C. Y. H., and X. L. X. analyzed the data and wrote the manuscript. X. P. L. and W. Y. G. carried out the DFT calculations. All authors discussed the results and commented on the manuscript.

Acknowledgements

This work was supported by the NSFC (Grant No. 21271117, 21371179, 21571187), NCET-11-0309, Taishan Scholar Foundation (ts201511019), and the Fundamental Research Funds for the Central Universities (13CX05010A, 14CX02150A, 20151066).

Notes and references

1 F. Perez-Ruiz, N. Dalbeth and T. Bardin, *Adv. Ther.*, 2015, **32**, 31.
2 Y. Gong, M. J. Wagner, J. Z. Li and M. J. Schnitzer, *Nat. Commun.*, 2014, **5**, 3674.
3 M. Kanbay, T. Jensen, Y. Solak, M. Le, C. Roncal-Jimenez, C. Rivard, M. A. Lanaspa, T. Nakagawa and R. J. Johnson, *Eur. J. Intern. Med.*, 2016, **29**, 3.
4 K. Tanaka and Y. Chujo, *NPG Asia Mater.*, 2015, **7**, 223.
5 J. Rebek, *Chem. Commun.*, 2000, 637.
6 Z. C. Hu, B. J. Deibert and J. Li, *Chem. Soc. Rev.*, 2014, **43**, 5815.
7 C. Liao, C. Mak, M. Zhang, H. L. Chan and F. Yan, *Adv. Mater.*, 2015, **27**, 676.
8 Q. Tang, Z. Y. Li, Y. B. Wei, X. Yang, L. T. Liu, C. B. Gong, X. B. Ma, M. H. W. Lam and C. F. Chow, *Mat. Sci. Eng. C-Mater.*, 2016, **66**, 33.
9 P. Xu, R. Li, Y. Tu and J. Yan, *Talanta*, 2015, **144**, 704.
10 D. Jin, M. H. Seo, B. T. Huy, Q. T. Pham, M. L. Conte, D. Thangadurai and Y. I. Lee, *Biosens. Bioelectron.*, 2016, **77**, 359.
11 E. Wajs, T. T. Nielsen, K. L. Larsen and A. Fragoso, *Nano Res.*, 2016, **9**, 2070.
12 A. S. Mahadevi and G. N. Sastry, *Chem. Rev.*, 2016, **116**, 2775.
13 M. C. Bellissent-Funel, A. Hassanali, M. Havenith, R. Henchman, P. Pohl, F. Sterpone, D. V. D. Spoel, Y. Xu and A. E. Garcia, *Chem. Rev.*, 2016, **116**, 7673.
14 T. J. Li, C. M. Chang, P. Y. Chang, Y. C. Chuang, C. C. Huang, W. C. Su and D. B. Shieh, *NPG Asia Mater.*, 2016, **8**, 277.
15 C. Tang, Z. S. Qian, Y. Y. Huang, J. M. Xu, H. Ao, M. Z. Zhao, J. Zhou, J. R. Chen and H. Feng, *Biosens. Bioelectron.*, 2016, **83**, 274.
16 H. Dong, Y. Y. Li, J. H. Yu, Y. Y. Song, X. J. Cai, J. Q. Liu, J. M. Zhang, R. C. Ewing and D. L. Shi, *Small*, 2013, **9**, 446.
17 Y. H. Li, X. R. Zhai, H. B. Wang, X. S. Liu, L. Guo, X. L. Ji, L. Wang, H. Y. Qiu and X. Y. Liu, *Microchim. Acta*, 2015, **182**, 1877.
18 D. Prochowicz, A. Kornowicz, I. Justyniak and J. Lewiński, *Coord. Chem. Rev.*, 2016, **306**, 331.
19 Y. H. Wei, D. Sun, D. Q. Yuan, Y. J. Liu, Y. Zhao, X. Y. Li, S. N. Wang, J. M. Dou, X. P. Wang, A. Y. Hao and D. F. Sun, *Chem. Sci.*, 2012, **3**, 2282.
20 J. Del Barrio, S. T. Ryan, P. G. Jambrina, E. Rosta and O. A. Scherman, *J. Am. Chem. Soc.*, 2016, **138**, 5745.
21 R. Zhao, C. Sandstrom, H. Zhang and T. Tan, *Mol.*, 2016, **21**, 372.
22 S. Park, S. Hwang, S. Takenaka and K. Kim, *Electroanal.*, 2015, **27**, 1159.
23 J. Park, Q. Jiang, D. Feng, L. Mao and H. C. Zhou, *J. Am. Chem. Soc.*, 2016, **138**, 3518.
24 X. L. Xin, J. X. Wang, C. F. Gong, H. Xu, R. M. Wang, S. J. Ji, H. X. Dong, Q. G. Meng, L. L. Zhang, F. N. Dai and D. F. Sun, *Sci. Rep.*, 2016, **6**, 21951.
25 B. Wang, X. L. Lv, D. Feng, L. H. Xie, J. Zhang, M. Li, Y. Xie, J. R. Li and H. C. Zhou, *J. Am. Chem. Soc.*, 2016, **138**, 6204.
26 Z. H. Hu, W. P. Lustig, J. M. Zhang, C. Zheng, H. Wang, S. J. Teat, Q. Gong, N. D. Rudd and J. Li, *J. Am. Chem. Soc.*, 2015, **137**, 16209.
27 A. Ojida, I. Takashima, T. Kohira, H. Nonaka and I. Hamachi, *J. Am. Chem. Soc.*, 2008, **130**, 12095.
28 L. Guo and D. Cao, *J. Mater. Chem. C*, 2015, **3**, 8490.
29 A. Hakonen, *Scientific World Journal*, 2013, **2013**, 624505.
30 A. Hakonen and N. Stromberg, *Analyst*, 2012, **137**, 315.
31 Y. J. Jang, O. G. Tsay, D. P. Murale, J. A. Jeong, A. Segev and D. G. Churchill, *Chem. Commun.*, 2014, **50**, 7531.
32 Q. Lu, J. Zhao, S. Xue, P. Yin, Y. Zhang and S. Yao, *Analyst*, 2015, **140**, 1155.
33 L. Wang, L. Yang, L. Li and D. Cao, *New J. Chem.*, 2016, **40**, 6706.
34 M. Yu, M. Shi, Z. Chen, F. Li, X. Li, Y. Gao, J. Xu, H. Yang, Z. Zhou, T. Yi and C. Huang, *Chem. – Eur. J.*, 2008, **14**, 6892.
35 H. Zhang, Q. Liu, T. Wang, Z. Yun, G. Li, J. Liu and G. Jiang, *Anal. Chim. Acta*, 2013, **770**, 140.
36 X. Yuan, M. I. Setyawati, A. S. Tan, C. N. Ong, D. T. Leong and J. P. Xie, *NPG Asia Mater.*, 2013, **5**, 39.
37 W. Chen, E. W. Rosser, D. Zhang, W. Shi, Y. L. Li, W.-J. Dong, H. M. Ma, D. H. Hu and M. A Xian, *Org. Lett.*, 2015, **17**, 2776.
38 H. K. Moon, M. Son, J. E. Park, S. M. Yoon, S. H. Lee and H. C. Choi, *NPG Asia Mater.*, 2012, **4**, 12.
39 K. S. Asha, R. Bhattacharjee and S. Mandal, *Angew. Chem., Int. Ed.*, 2016, **55**, 11528.
40 S. Y. Ding, M. Dong, Y. W. Wang, Y. T. Chen, H. Z. Wang, C. Y. Su and W. Wang, *J. Am. Chem. Soc.*, 2016, **138**, 3031.
41 K. Mariappan, M. Alaparthi, M. Hoffman, M. A. Rama, V. Balasubramanian, D. M. John and A. G. Sykes, *Dalton Trans.*, 2015, **44**, 11774.
42 X. Ma and Y. Zhao, *Chem. Rev.*, 2015, **115**, 7794.
43 R. Q. Paulpandi, S. Ramasamy, M. S. Paulraj, F. G. D. Baños, G. Villora, J. P. Cerón-Carrasco, H. Pérez-Sánchez and I. V. M. V. Enoch, *RSC Adv.*, 2016, **6**, 15670.
44 X. L. Li, Q. Shi, W. Jin, G. Li, K. Todoroki, H. Mizuno, T. Toyo'oka and J. Z. Min, *Biomed. Chromatogr.*, 2016, **30**, 1338.
45 J. P. Perdew and Y. Wang, *Phys. Rev. B*, 1992, **45**, 13244.
46 B. Delley, *J. Chem. Phys.*, 2000, **113**, 7756.
47 V. Veeramani, R. Madhu, S. M. Chen, B. S. Lou, J. Palanisamy and V. S. Vasantha, *Sci. Rep.*, 2015, **5**, 10141.
48 N. Misra, V. Kumar, L. Borde and L. Varshney, *Sens. Actuators B.*, 2013, **178**, 371.
49 C. Yuan, Z. Jin and X. Xu, *Carbohyd. Polym.*, 2012, **89**, 492.
50 Z. Moussa, M. Hmadeh, M. G. Abiad, O. H. Dib and D. Patra, *Food Chem.*, 2016, **212**, 485.

